

## CHAPTER 4 - CYCLIC LOAD TESTING OF SEMI- INTEGRAL BRIDGE ABUTMENTS

### 4.1. Introduction

The Virginia Department of Transportation (VDOT) has developed a semi-integral abutment detail as seen in Figure 4.1. This abutment is expected to rotate over the pile cap. This rotation helps reduce the pile stresses by reducing the lateral displacement of the foundation piles and by reducing the moments transferred from the superstructure.

The objective of the experimental research program presented in this chapter is threefold. The first objective is to investigate the potential problems of the VDOT semi-integral abutment and recommend modification for design. The second objective is to evaluate the rotational stiffness of the semi-integral abutment. The third objective is to investigate the ability of the semi-integral abutment to withstand cyclic loading induced by temperature variations during the expected life span of the bridge.

A potential problem in the original detail of the semi-integral abutment was discovered during static testing. Upon consultation with the Staunton office of VDOT, a revised detail was developed by that office. The revised detail is illustrated in Figure 4.2. The abutment with the revised detail was also subjected to the same testing program as the original detail.

## 4.2. Design and Construction

Standard design plans of VDOT were used to establish the size of the specimens. The Staunton office of VDOT provided the information necessary for design, and reviewed the plans before construction. Construction plans of the semi-integral abutments can be seen in Appendix B.

The specimens were constructed in the structures laboratory of Virginia Tech. Reinforcements for the specimens were prefabricated by Resco Steel of Salem, VA. The concrete was provided by New River Concrete of Blacksburg, VA. The building of formwork and other tasks for the construction of the abutment blocks were conducted by the technicians at the structures laboratory of Virginia Tech.

Dimensions of the specimens were selected to take full advantage of the layout of the reaction floor in the lab. The reaction floor consists of parallel steel beams spaced 8-feet apart. Pre-existing holes every 2-feet on the reaction beams were used to mount the test specimens onto the reaction floor. The crane capacity at the structures laboratory is 10,000 lbs.

The Virginia Transportation Research Council (VTRC) supplied the dowels needed for building the specimens. The dowels were manufactured by the Charlotte steel mill of Ameristeel.

Concrete slump from each batch was checked before placing the concrete. Concrete cylinders from each batch were taken to measure the strength on the test day.

Two specimens with the original detail as illustrated in Figure 4.1 were constructed. The construction took place between November 1999 and January 2000. The pile cap block and the abutment block of the first specimen (Specimen A) were cast on November 23, 1999 and December 8, 1999, respectively. Similarly, the pile cap block and the abutment block of the second specimen (Specimen B) were cast on November 29, 1999 and January 5, 2000, respectively. Figure 4.3 presents photographs from the construction.

During static load tests of the first two specimens, a deficiency in the design was discovered. Upon consultation with the Staunton office of VDOT, a revised detail as illustrated in Figure 4.2 was developed by that office. The construction of the revised

detail was completed in May 2000. The pile cap block of Specimen B was re-used. After removing the abutment of Specimen B, the surface of the pile cap was leveled and cleaned. One of the dowels was damaged during the removal of the abutment. A new dowel was driven inside the existing hole into the pile cap. Epoxy was placed inside the hole before the dowel was driven in to assure proper bonding between the concrete and the dowel. The revised detail was built on the surface of this recycled pile cap. Figure 4.4 presents photographs from the construction of the revised detail (Specimen C).

### 4.3. Material properties

#### 4.3.1. Dowels

The dowels were manufactured by the Charlotte steel mill of Ameristeel. They had yield and tensile strengths of 49,530 psi and 73,030 psi, respectively, as tested according to ASTM A36-94 by the manufacturer.

#### 4.3.2. Concrete

The specimens were cast from locally purchased VDOT class A4 concrete. This type of concrete has a minimum 28-day strength of 4,000 psi,  $6.5 \pm 1.5\%$  air content, and a minimum cement content of 600 lbs per cubic yard of concrete. Coarse non-polishing aggregate was used.

Concrete slump was checked for each batch received before placing the concrete. The slump varied from 3-½ to 4 inches. Concrete samples from each batch were collected and compressive strengths of these samples were determined on the day of testing. Compressive strength and other useful properties of concrete for each member of the specimens are summarized in Table 4.1. Young's modulus of the concrete is calculated by  $E = 57,000\sqrt{f'_c}$ , where  $f'_c$  is the strength on the test day in psi. Additional concrete samples were taken to establish the strength increase of the concrete over time. Variation of the strength of the concrete with time is portrayed in Figure 4.5.

**Table 4.1.** Strength properties of concrete

| Member                | 28-day strength (psi) | Age of concrete on test day (days) | Test-day strength (psi) |
|-----------------------|-----------------------|------------------------------------|-------------------------|
| Specimen A – pile cap | 5,970                 | 69                                 | 6,920                   |
| Specimen A – abutment | 6,400                 | 58                                 | 7,740                   |
| Specimen B – pile cap | 6,290                 | 120                                | 7,480                   |
| Specimen B – abutment | 6,370                 | 83                                 | 7,380                   |
| Specimen C – pile cap | 6,290                 | 196                                | 7,800                   |
| Specimen C – abutment | 5,530                 | 10                                 | 4,420                   |

#### 4.4. Load Test Setup

The setup of the load tests consists of four tasks:

1. Mounting the specimens onto the reaction floor,
2. Application of the vertical load,
3. Application of the lateral load in static loading, and
4. Application of the lateral load in cyclic loading.

##### 4.4.1. Mounting specimens on reaction floor

Three threaded rods were placed in each pile cap during construction such that the rods extend out of the cap. On each side of a pile cap, an 8-foot segment of a HP10x42 is bolted on the threaded rods that are protruding from the pile cap. Figure 4.6 shows the locations of the threaded rods, and the floor-mounting plan of the pile caps. The HP10x42 segments were bolted down to the reaction floor at each corner by four threaded steel rods.

#### 4.4.2. Application of vertical load

The application of the vertical load was achieved through a specially designed system. The system consists of three components:

1. A stiff steel frame,
2. A single-acting hydraulic ram, and
3. A constant pressure valve

The stiff steel frame was built around the specimens as pictured in Figure 4.7 to support the vertical loading ram. Loads were applied by a single-acting hydraulic ram. A compression load cell was placed between the frame and the ram.

As the lateral loads are applied and removed, the specimen rotates and moves up or down under the ram. This up and down movement of the sample makes it impossible to maintain a constant vertical load if a standard ram is used. An Enerpac V-152 relief valve was used to maintain a constant load. The relief valve is originally designed to limit the applied load. The valve serves as a constant pressure valve by letting the pump run throughout the test. When the specimen raises under the ram, the valve relieves the extra pressure as soon as the maximum preset pressure is reached. When the abutment is lowered under the ram, the continuously running pump equilibrates the pressure to the preset pressure of the relief valve. The combination of using the relief valve and keeping the pump running allowed maintaining the vertical load constant within  $\pm 10\%$  of the target value.

A roller and tilting-plate mechanism was placed between the specimen and the vertical load ram in order to minimize the lateral load transfer at this location. A picture of this assembly is presented in Figure 4.8.

#### 4.4.3. Application of lateral load in static loading

A manually controlled hydraulic ram capable of applying 50 kips of load was used to apply the static lateral loads. A view of the setup used is pictured in Figure 4.9. Support for the ram was provided by an A-shaped large stiff frame. A 50-kip tension load cell

was placed between the ram and the specimen to monitor the lateral load. The system was designed only to pull the specimen.

#### *4.4.4. Application of lateral load in cyclic loading*

A computer controlled MTS hydraulic actuator capable of applying  $\pm 50$  kips of load and  $\pm 3$  inches of displacement was used to impose cyclic lateral loads. Support for the ram was provided by the same A-shaped large frame used in the static load tests. A view of the actuator during testing is shown in Figure 4.10. The system was capable of applying both push and pull forces.

The actuator can be used with either load or displacement control. Actuator control was provided by a MTS 458.10 MicroConsole unit with a 458.14 AC displacement controller, a 458.12 DC load controller, and a 458.90 function generator. All tests were run displacement controlled.

#### *4.4.5 Instrumentation and Data Acquisition*

Data acquisition during the static testing of Specimen A and Specimen B was performed by System 4000 marketed by Measurements Group. The system includes a unit to read the analog voltage readings and to convert them into digital signals. The measurements are then stored into a personal computer.

Data from measuring devices during cyclic tests of Specimen B were collected into a MEGADAC 3108AC unit made by Optim Electronics. The unit converts the analog voltage readings from the measuring devices into digital signals. Digital signals are then sent to a PC, from which signals are read by the TCS data acquisition software. This setup is also used during the static and cyclic testing of the revised semi-integral abutment (Specimen C).

Three types of measuring devices were used:

1. Displacement
2. Load
3. Strain

Displacement measurements were made by wire pot transducers. Each transducer was calibrated on-site right before it was put into service. Five transducers were used during each test. For convenience, the locations of the transducers were kept the same in all tests. Three of these transducers measured the lateral displacements of the abutment while the remaining two were used to record the vertical displacement of the abutment at the top. Figure 4.11 shows the locations of the displacement measuring devices.

In addition to displacement transducers, the MTS actuator has a built-in LVDT to measure the displacement of the actuator. Readings of this LVDT reflect the combined displacement of the abutment at the location where the load is applied to the specimen and the displacement at the support of the actuator.

Two load cells were used: one for measuring the lateral load and one for measuring the vertical load. The lateral load cell used during cyclic loading was built into the MTS actuator. This load cell, capable of measuring both tension and compression loads, was used to measure the lateral load transferred to the abutment. During static loading a 50-kip tension load cell was used to monitor the lateral loads applied to the specimens. The other load cell was a compression load cell, which was used to monitor the vertical loads applied to the abutment. Calibrations were checked before using these load cells, and no misreading was found.

Strain gages were purchased from the Measurements Group and installed by the manufacturer's instructions. CEA-06-250UN-120 gages were used on steel dowel surfaces. The steel gages were  $\frac{1}{4}$  in. long and had 120-ohm resistance with a gage factor of 2.065. The gages were placed on the opposite surface of each dowel instrumented to monitor bending stresses. The elevation of the strain gages was the same as the joint filler material. Four of the six dowels used per specimen were instrumented with strain gages for Specimens A and B. Two of the dowels of Specimen C were instrumented with strain gages.

#### **4.5. Test Program**

The purpose of the test program was to investigate the VDOT semi-integral abutment hinge by performing static and cyclic load tests in order to evaluate the

rotational stiffness and cyclic loading damage potential of this type of abutment. Two specimens were built to conduct the experiments.

In the first static loading test of the first abutment, the shear key had unexpectedly failed. The shear key of the second abutment had also failed in the same manner at exactly the same lateral load. Upon consultation with the Staunton office of VDOT, a revised detail was developed by that office. The revised detail can be seen in Figure 4.2. A third specimen based on the detail shown in Figure 4.2 was built. The revised detail did not show any failure mechanism.

Static and cyclic load tests were conducted after the shear key failure of the first two specimens (Specimen A and Specimen B). For all specimens, static load tests preceded the dynamic load tests. Complete details of the static and cyclic load testing are presented below.

#### *4.5.1. Static Testing*

All three of the semi-integral abutments were subjected to static lateral loading so that the top of the abutment displaces about an inch. A limit for the lateral load was set as 40 kips, which was imposed by the capacity of the load frame used to support the ram. The lateral loads were applied 5 inches below the top of the abutment or 31 inches above the abutment/pile cap joint. All three specimens were tested under vertical loads of 0, 35, and 70 kips.

Three additional tests were conducted on Specimen B by applying the lateral load 14 inches below the top of the abutment for vertical loads of 0, 35, and 70 kips.

In total, twelve static tests were conducted. Data obtained can be used to determine the rotational stiffness of the specimens.

#### *4.5.2. Application of displacement cycles*

Cyclic load tests were conducted on specimens B and C for the purpose of simulating the effects of lateral loading induced by temperature changes over the

expected life of the bridge. The life span of an integral bridge was specified to be 75 years.

Cyclic displacements were applied according to the method proposed in Chapter 3. Maximum displacements at the top of the abutment were set as  $\pm 0.5$  inches. Table 4.2 shows the displacement pattern used to simulate 75 years of thermal bridge displacements. Data collection was performed right after the 10<sup>th</sup>, 50<sup>th</sup>, and 75<sup>th</sup> years of simulated time. After the initial recording of data, ten-years of temperature effects were imposed according to the displacement pattern shown in Table 4.2. The number of displacement cycles in Table 4.2 was multiplied by ten. Forty more years of cyclic loading was imposed in the same manner. Finally, twenty-five more years of displacements were applied to complete the test.

Two different vertical loads were used for each specimen: 0 and 35 kips. In total, four cyclic loading tests were conducted on two slightly different types of semi-integral abutments.

**Table 4.2.** Representation of temperature-induced displacement cycles for one year for a maximum expected displacement range from -0.5 to +0.5 inches.

| Group No | Corresponding days | Mean displacement level at the top of abutment (in) | Magnitude of cycles (in.) | Number of cycles for one year |
|----------|--------------------|---|---------------------------|-------------------------------|
| 1        | 0-46               | -0.375  | 0.25                      | 46                            |
| 2        | 46-91, 320-365     | -0.188  | 0.25                      | 91                            |
| 3        | 91-135, 270-320    | 0.000   | 0.25                      | 91                            |
| 4        | 135-180, 225-270   | 0.188   | 0.25                      | 91                            |
| 5        | 180-225            | 0.375   | 0.25                      | 46                            |
| 6        | seasonal           | 0.000   | 1.00                      | 1                             |

#### **4.6. Shear Key Failure**

In the first static test of Specimen A, the shear key of the specimen failed with a loud noise. At the time of the failure, the lateral was about 34 kips applied 29 inches above the shear key. No vertical load was applied to the sample other than its self-weight. A picture of the failed shear key is shown in Figure 4.12.

Analysis of the data indicates that the abutment and the pile cap rotated as a single structural unit prior to failure of the shear key. This suggests that the cold bond between the pile cap and the abutment was as strong as if they were cast together. The lateral load at the time of failure was calculated to generate a tensile stress of about 550 psi in the concrete of the shear key. This stress is within the estimated tensile strength range of the specimen.

Specimen B was also tested under exactly the same conditions as the first specimen. The failure of the shear key was observed to take place in a similar manner when the lateral load reached about 34 kips applied 28 inches above the shear key. Tensile stresses generated by the lateral load are within the tensile strength range of the concrete.

It was concluded that the failure of the shear key was due to concrete of the shear key failing in tension due to bending. Static load tests were conducted after the shear key failure and found that both abutments were able to provide shear resistance, assuring that the dowels did not fail and the failure was limited to the concrete of the shear key. Unfortunately, all of the strain gages were lost at the time the shear key failed.

#### **4.7. Results of Static Load Tests**

The results of the static load tests are presented below in three groups. The first group presents the lateral load/displacement relationships under various vertical loads. In the second group, the variation of the point of rotation of the abutment under various loading conditions is presented. Finally, the rotational stiffness of the specimens is documented.

#### 4.7.1. Lateral load displacement relationship

As the lateral loads were applied to the specimens, the abutment rotated over the pile cap. Displacement transducers indicated that the pile caps experienced a small amount of rotation as well. The relative displacements of the abutments were calculated by subtracting the displacement readings measured at the top of the pile cap from the readings of the two displacement transducers used to monitor the displacements of the abutments at two different heights. By taking the average values of these two relative displacement values of the abutment and assuming a rigid behavior for the abutment, the relative displacement [with respect to the pile cap] at the top of the abutment was calculated.

The relationship between the lateral load and the relative displacement at the top of the abutment is shown in Figures 4.13, 4.14, and 4.15 for Specimens A, B, and C, respectively. Figures 4.13 and 4.15 contain three load/displacement curves for the vertical loads of 0, 35, and 70 kips applied on the abutments to simulate the dead load of the bridge. In Figure 4.14, lateral load/displacement responses of the abutment are shown for two different points of lateral load application. Half of the data shows the response of the abutment under three levels of vertical load (0, 35 and 70 kips) when the lateral load was applied 31 inches above the top of the pile cap. The other half of the data shows the response of the abutment under three levels of vertical load (0, 35 and 70 kips) when the lateral load was applied 22 inches above the top of the pile cap. As seen in the figures, the loading/unloading curves for the original semi-integral abutment hinge (Specimen A and Specimen B) are much closer to each other than the loading/unloading curves of the revised detail (Specimen C).

Lateral load/displacement relations of Specimen A and Specimen B are portrayed in Figure 4.16. As seen in the figure, the behavior is almost identical for zero vertical load. For other vertical loads, Specimen A consistently has higher lateral load response for a given displacement. This may be due to the fact that the irregular failure surface of the shear key caused the two abutments to have different points of rotation for the same lateral displacement at the abutment. Another factor could be that the roller and the

tilting-plate assembly used under the vertical loading ram provided different resistance for the two specimens, resulting in different lateral loads for a given displacement.

Figure 4.17 and Figure 4.18 compare the response of the revised abutment detail (Specimen C) to Specimen A and Specimen B, respectively. It is clear that the initial response of the revised abutment is stiffer than that of the other two specimens for zero vertical loading. Because of the discrepancy between Specimen A and Specimen B for other values of vertical loads, the trend in load response between the initial and the revised semi-integral abutment is not clear.

Bending strains of the dowels were recorded during static loading of Specimen C under various vertical loads and presented in Figure 4.19. Strains were averaged from all channels and were plotted against the relative lateral displacement of the top of the abutment. As seen in the figure, the strain/displacement relationship is approximately linear. The maximum strain measured during the tests is about 50 % of the yield strain of the dowels. The yield strain of the dowels is slightly over 1,400  $\mu\epsilon$ . Bending strains of the test when the vertical load was 70 kips are about 10% higher than other two tests.

#### *4.7.2. Point of rotation of abutments*

As the abutment was subjected to lateral displacements, it rotated over the pile cap. The point of rotation moves because of the compressibility of the joint filler between the pile cap and the abutment. From the two vertical displacement readings measured in the front and on the backside of the abutment, the point of rotation can be calculated because the abutment rotates as a rigid body.

Variations of the point of rotation as a function of the relative displacement at the top of the abutment are presented in Figures 4.20, 4.21, and 4.22 for Specimens A, B, and C, respectively. The point of rotation was calculated with respect to the center of the abutment, i.e., a value of zero means that the abutment is rotating about its middle point while a value of 15 in. means that the abutment is rotating around its edge. As seen in the figures, the point of rotation moves towards the edge of the abutment as it is pulled, and moves back towards the center as the specimen is unloaded. The behavior of Specimen C is noticeably different from the behavior of the other two specimens. Specimen A and

Specimen B show similar rotational behavior, although a difference is observable. This difference in the behavior is probably responsible for the difference seen in their lateral load/displacement responses presented in Figure 4.16.

#### 4.7.3. Rotational stiffness of specimens

Rotational stiffness of the specimens was calculated as the ratio of the moment around the point of rotation to the rotation of the abutment. Variations of the rotational stiffness as a function of the relative displacement at the top of the abutment are presented in Figures 4.23, 4.24, and 4.25 for Specimens A, B, and C, respectively.

As seen in these figures, rotational stiffness decreases with increasing rotations of the abutments. The initial values of the rotational stiffness for Specimens A and B are higher than those of Specimen C. However, at higher rotations all values are converging to a constant of around 20,000 in-kip/radians. The figures also indicate that the abutments have higher rotational stiffness with higher vertical load, though the effect of the vertical load is not significant.

## 4.8. Results of Cyclic Load Tests

Cyclic load tests were carried out following the static load tests on Specimen B and Specimen C. Each specimen was tested under 0 and 35 kip vertical loads. Tests were conducted as displacement controlled according to Table 4.2. Data was collected at the beginning of the test, after the 10<sup>th</sup> year, the 50<sup>th</sup> year, and the 75<sup>th</sup> year of simulated time. Only the data of the first and the last cycles will be shown for clarity of the graphs.

Figure 4.26 shows the lateral load hysteresis loops for Specimen B under zero vertical load while Figure 4.27 shows a similar graph for the same specimen under a vertical load of 35 kips. The latter figure shows half the loops of the data because the data on the other half was unreliable as it was affected by external factors. As seen in these figures, the damage introduced by over 27,000 cycles is almost non-existent.

Figure 4.26 indicates no damage at all while Figure 4.27 indicates some softening in load response for 35-kip vertical loading.

Lateral load hysteresis loops for Specimen C under 0- and 35-kip vertical loads are shown in Figures 4.28, and 4.29, respectively. As evident in both figures, there is no sign of damage. The load/displacement behavior of the specimen is virtually unchanged after 75-years of displacement cycles. Bending strains of the dowels also show no change in response with cyclic loading as depicted in Figures 4.30 and 4.31 for 0- and 35-kip vertical loading, respectively.

Specimen C was also subject to 150 cycles consisting of  $\pm 2.5$  inch displacements cycles at the top of the abutment after the completion of the previous cyclic test program in an attempt to fail the dowels. The lateral load and the bending strain responses of the specimen are presented in Figures 4.32 and 4.33, respectively. No vertical load was applied to the specimen. Only the responses of the first and the 150<sup>th</sup> cycles are shown in these figures. Even at these higher rotations, the specimen was able to handle the loads with no sign of damage. The maximum bending strain seen in Figure 4.33 is slightly higher than the yield strain ( $\sim 1,400 \mu\epsilon$ ) of the dowels.

#### **4.9. Conclusions and Recommendations**

The original VDOT semi-integral abutment hinge experienced shear key failure as observed in two large-scale laboratory tests. The revised hinge detail did not exhibit this behavior.

As the specimens were subjected to lateral loading, the abutments rotated at their base over the pile cap. The point of rotation appears to be a function of the vertical load, the amount of abutment rotation, and the compressibility of the joint filler.

The rotational stiffness of the abutments appears to be a function of the abutment rotation. At higher rotations, the rotational stiffness appears to converge to a low constant. Thus, it can be concluded that the semi-integral abutments can significantly reduce the moments transferred from the superstructure down to the foundation piles.

Failure of the shear key for existing bridges supported by semi-integral abutments with a shear key might be a concern. However, a catastrophic failure of an integral bridge is not anticipated because of a shear key failure as the subsequent static and cyclic tests indicated that the specimens behaved well by tolerating over 27,000 cycles without further damage.

The revised semi-integral abutment detail showed no sign of damage. It tolerated 75-years of displacement cycles without any appreciable change in its behavior. The revised detail was also able to tolerate very large displacement cycles without damage. During these displacement cycles, the maximum bending strain in the dowels was slightly over the yield strain of the dowels.

Semi-integral abutments are recommended for longer integral bridges because they can reduce pile stresses. As the need to build longer integral bridges grows, the role of the semi-integral abutments is expected to become more important.

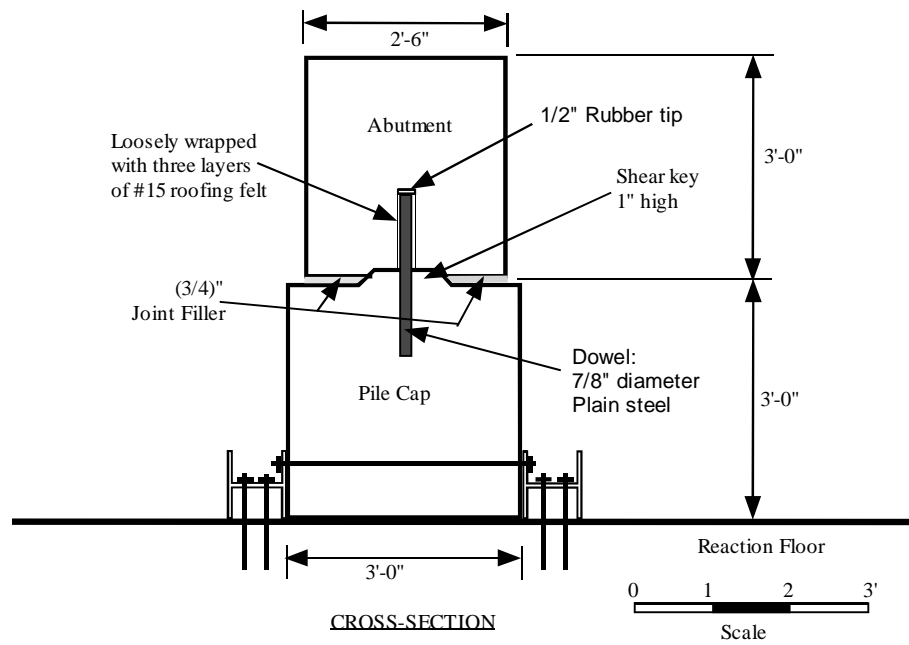


**Figure 4.1.** Schematic illustration of the initial VDOT semi integral abutment hinge

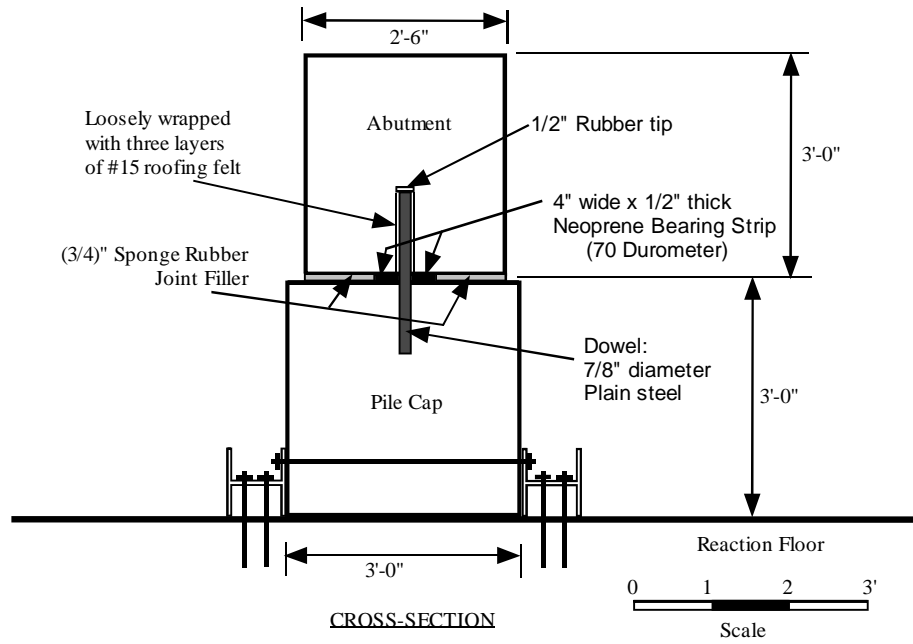


**Figure 4.2.** Schematic illustration of the revised VDOT semi integral abutment hinge



**Figure 4.3.** Pictures from construction of the initial VDOT semi integral abutment hinge



**Figure 4.4.** Pictures from construction of the revised VDOT semi integral abutment hinge

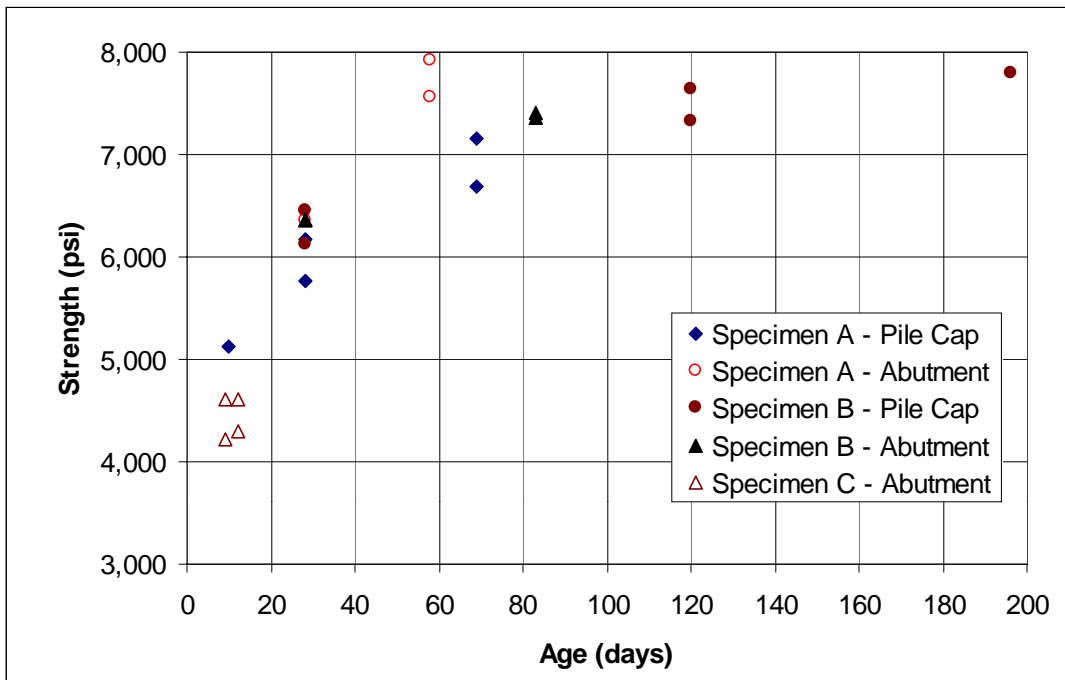


**Figure 4.5.** Increase in strength of concrete with time

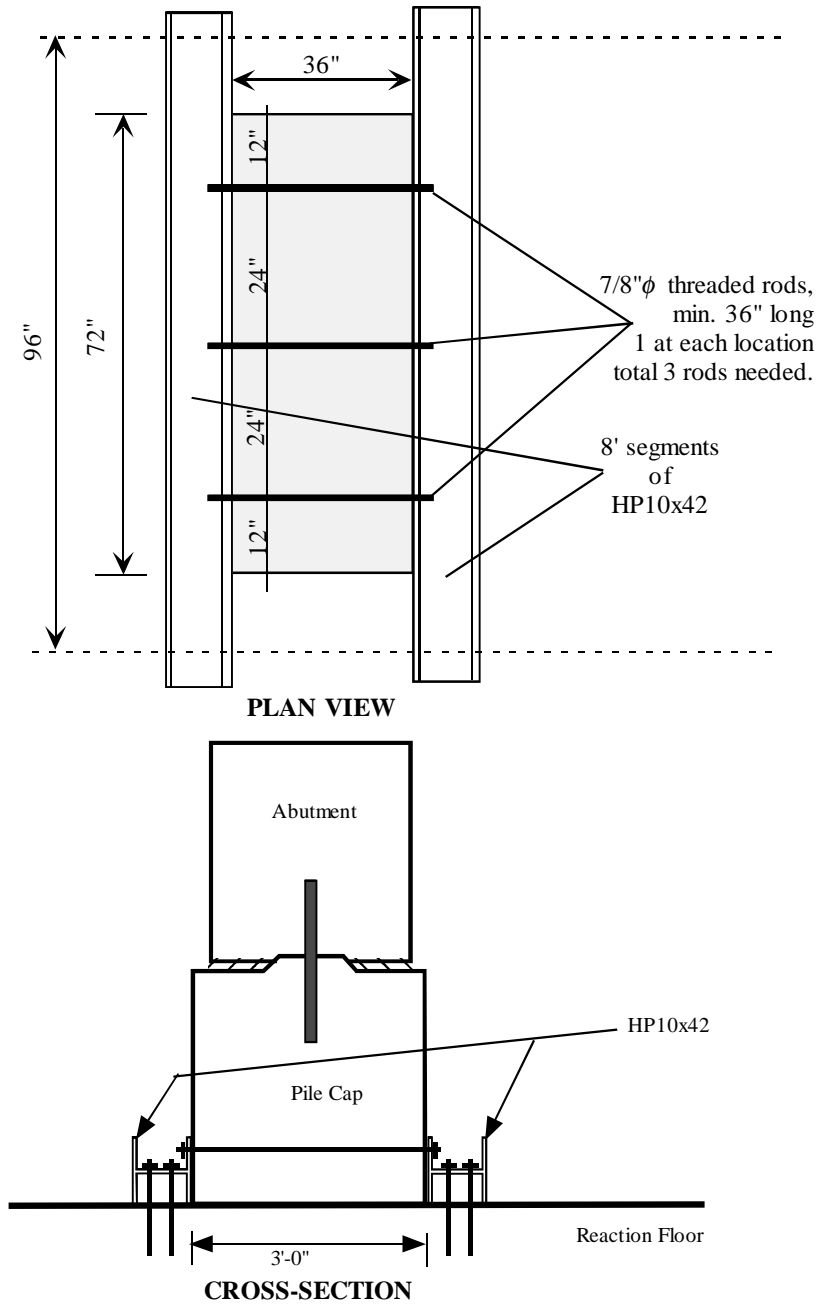


**Figure 4.6.** Schematic illustration of mounting pile caps on reaction floor



**Figure 4.7.** Setup used to apply vertical load to specimens



**Figure 4.8.** Roller and tilting-plate assembly used between ram and specimen

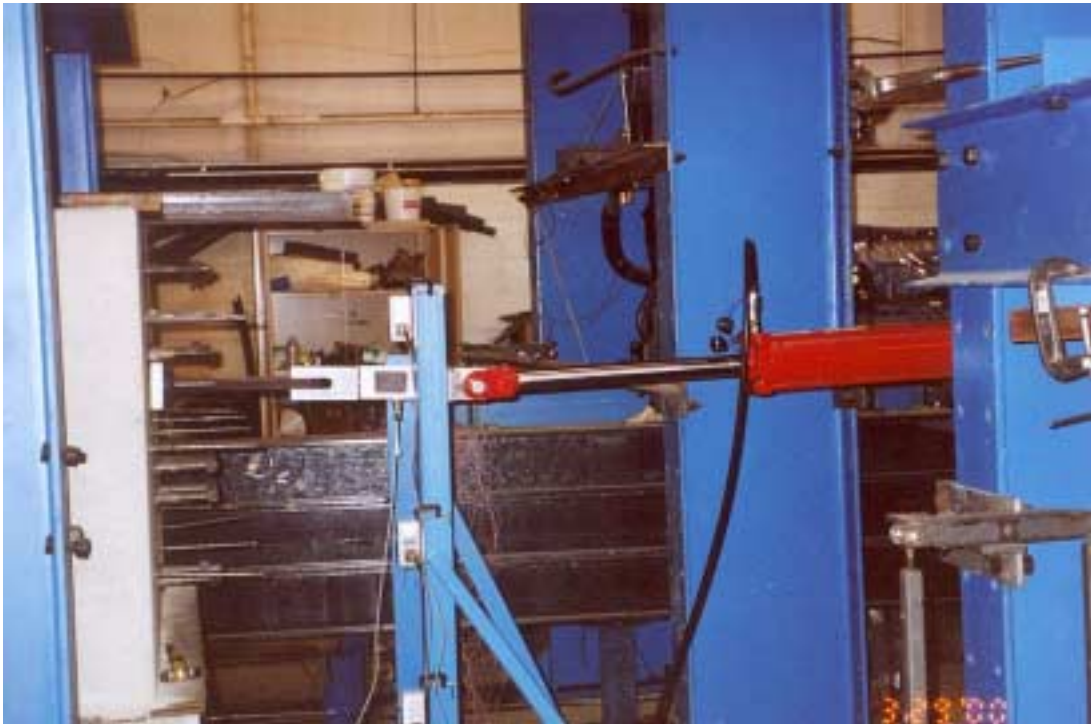


**Figure 4.9.** Setup used to apply static lateral load



**Figure 4.10.** Setup used to apply cyclic lateral load

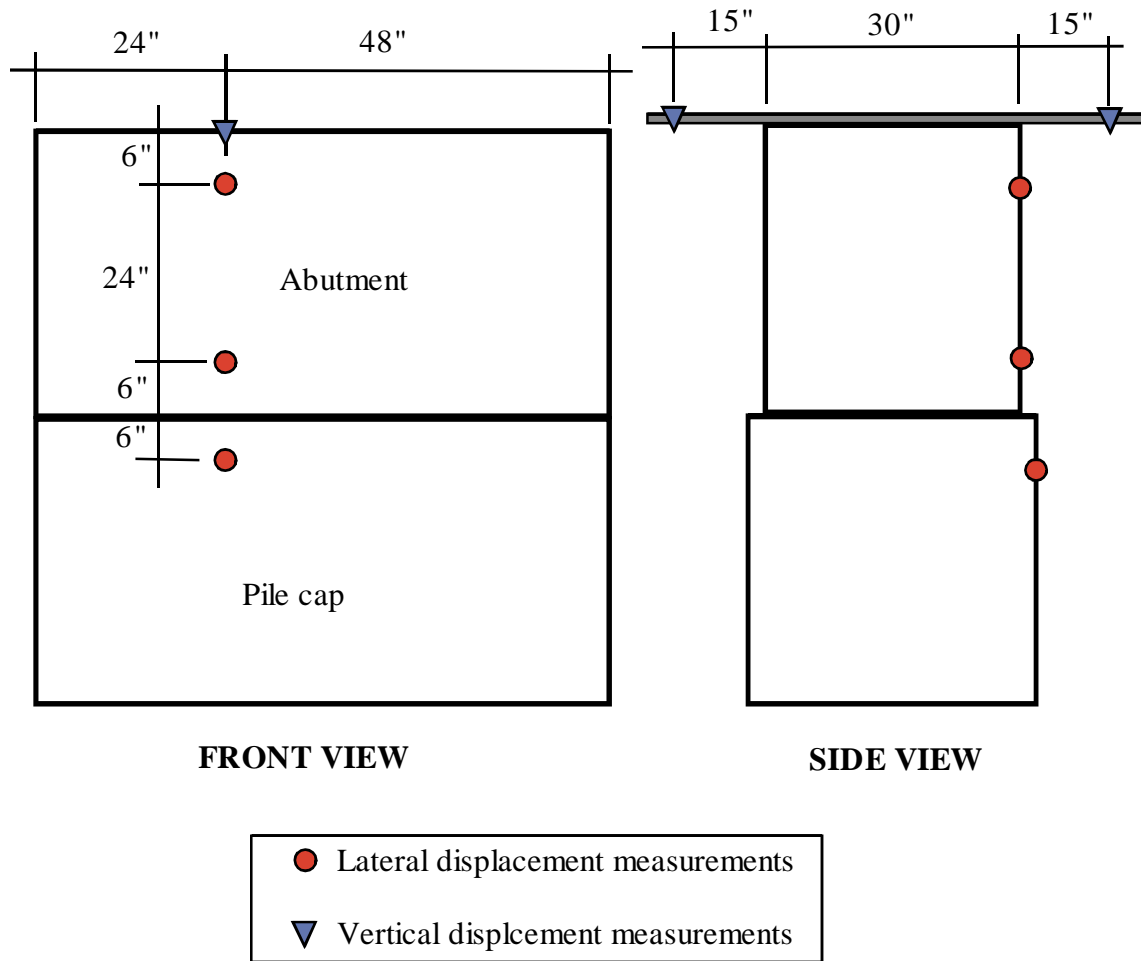


**Figure 4.11.** Locations of displacement measuring devices



**Figure 4.12.** Picture of failed shear key

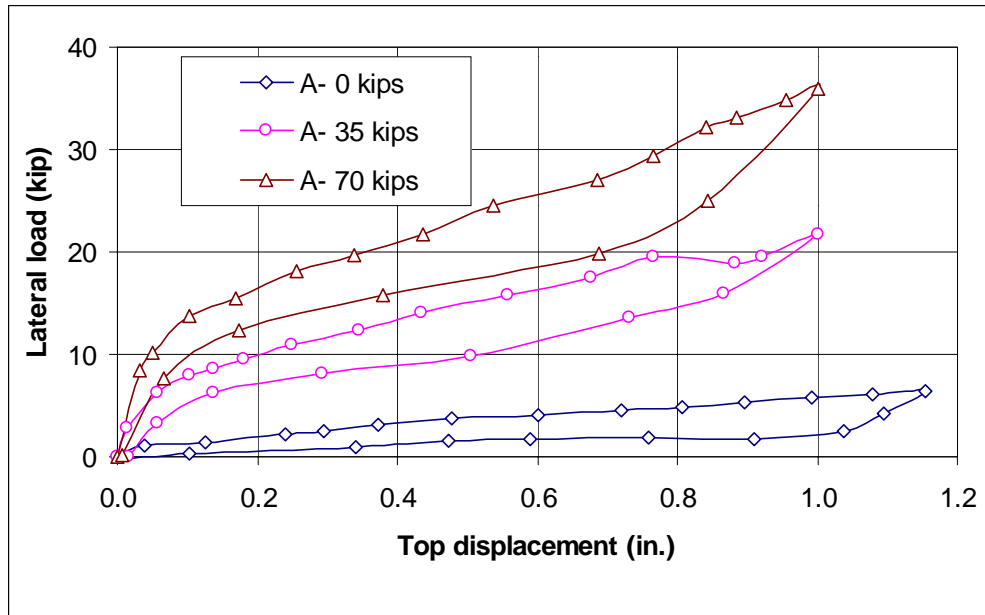
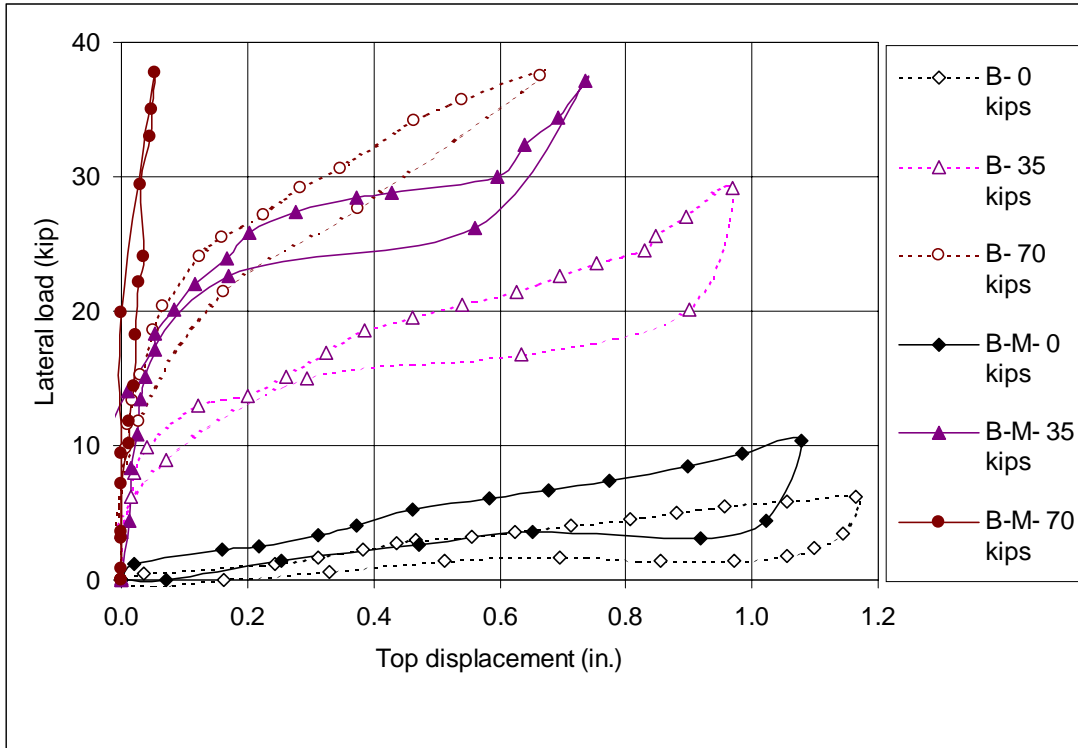


Figure 4.13. Lateral load/displacement relation of Specimen A for various vertical loads



**Figure 4.14.** Lateral load/displacement relation of Specimen B for various vertical loads

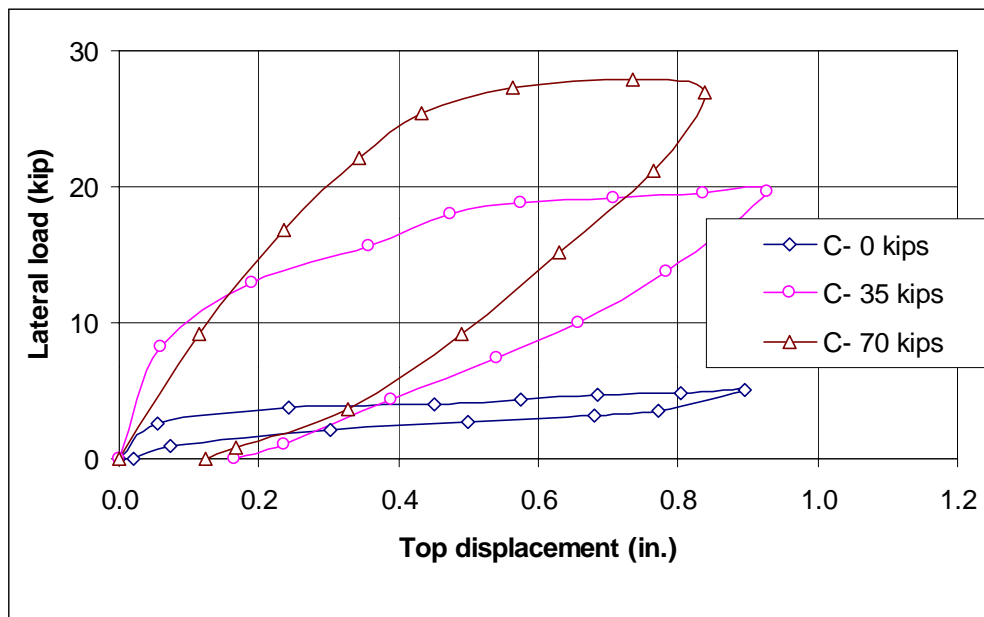
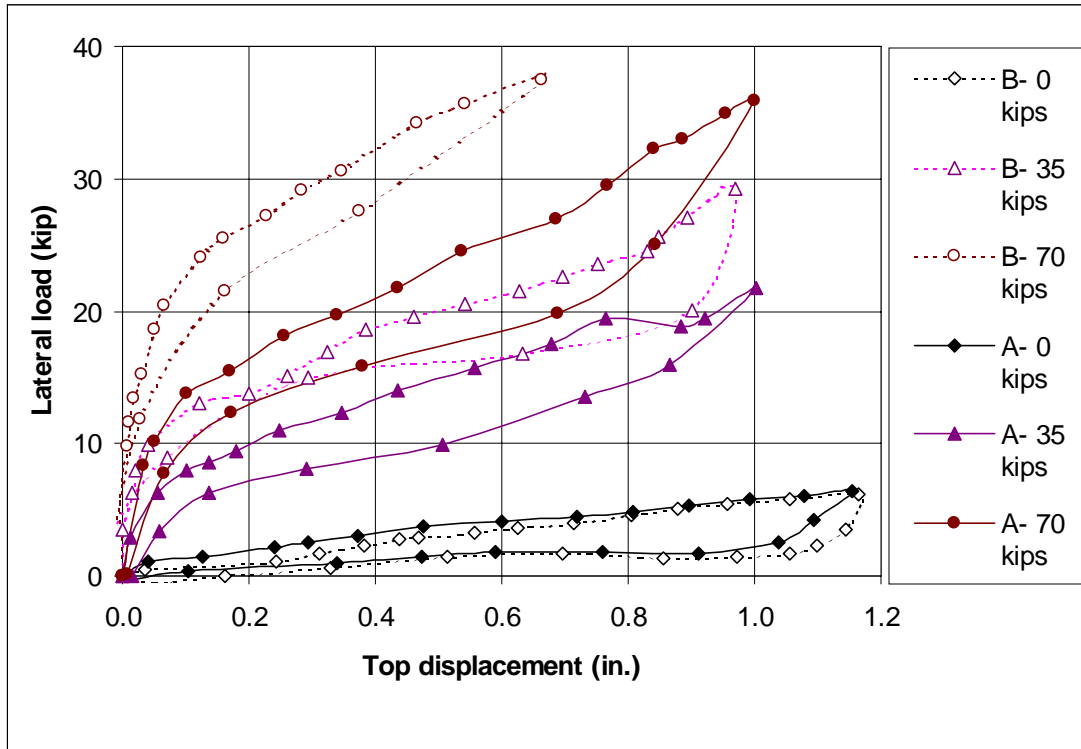


Figure 4.15. Lateral load/displacement relation of Specimen C for various vertical loads



**Figure 4.16.** Comparison of lateral load/displacement relations of Specimens A and B

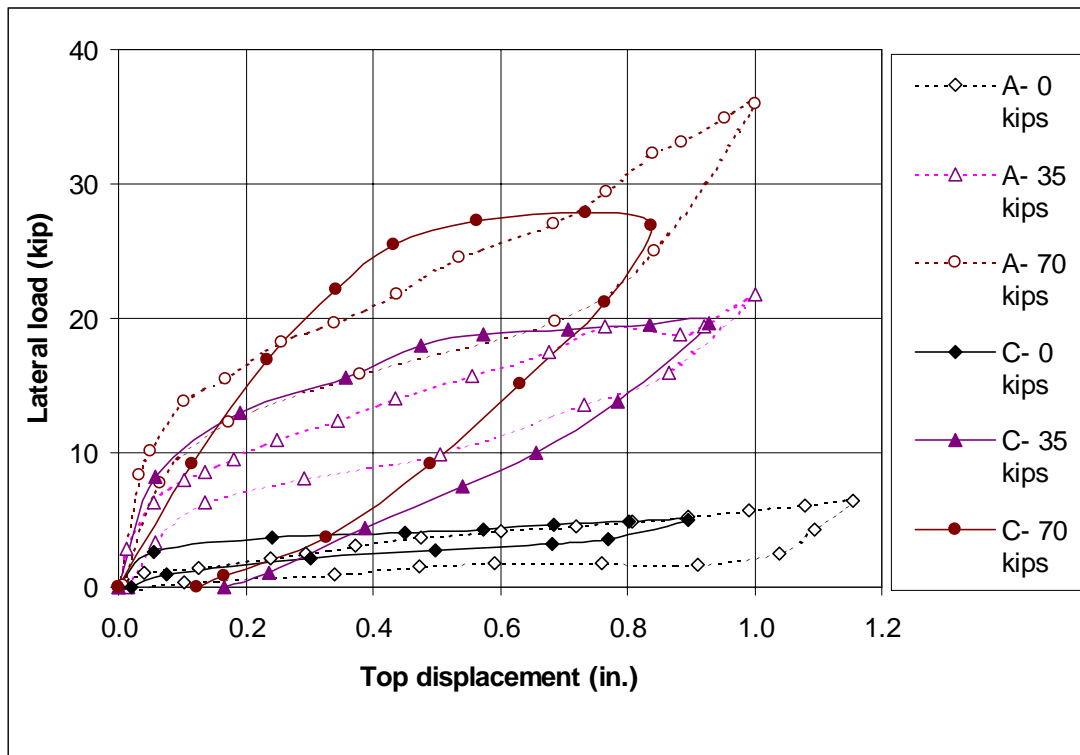


Figure 4.17. Comparison of lateral load/displacement relations of Specimens A and C

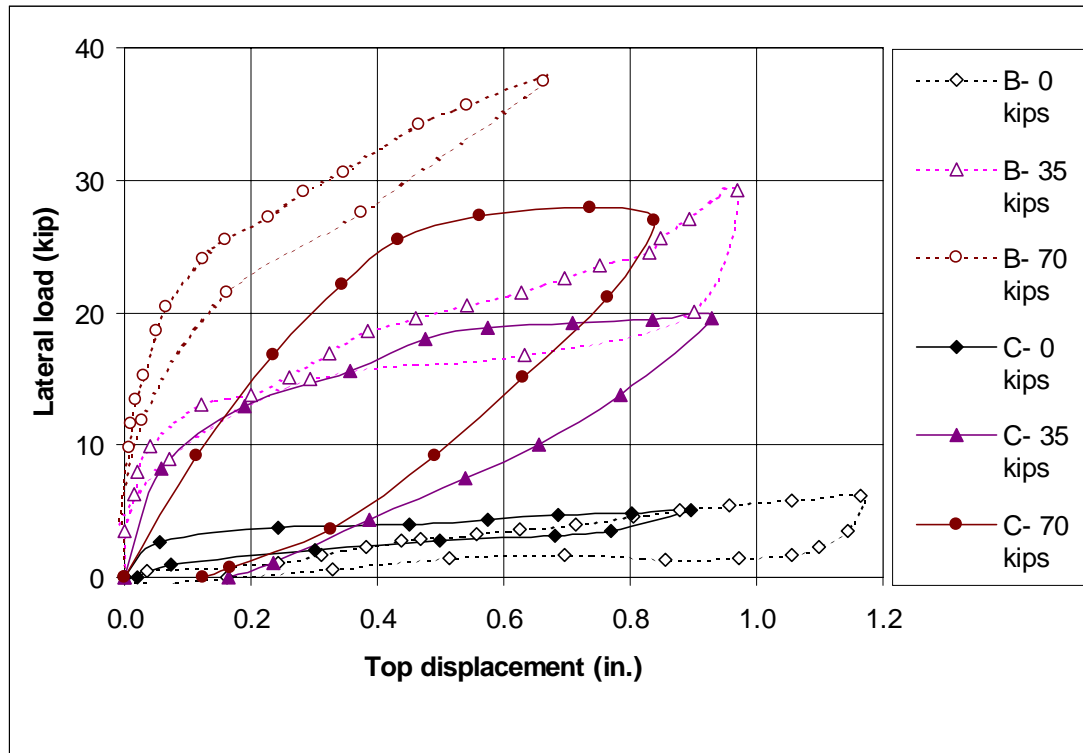
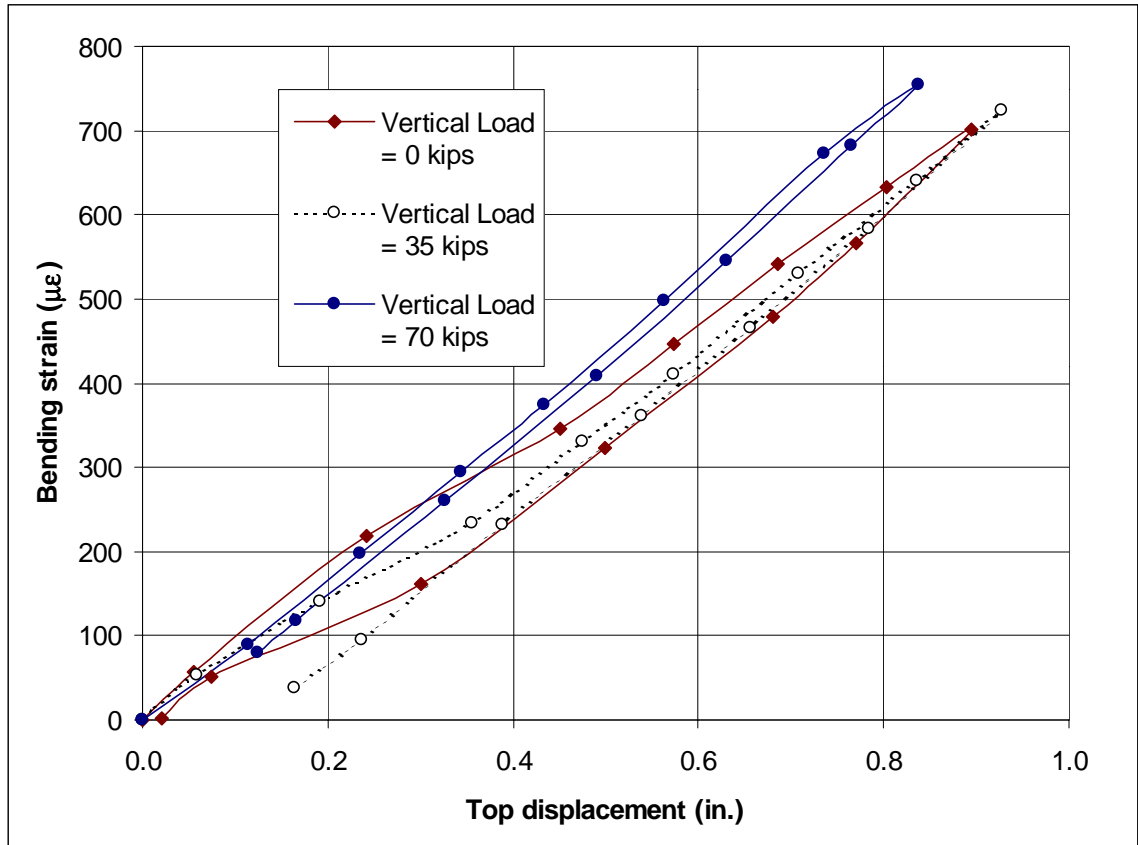
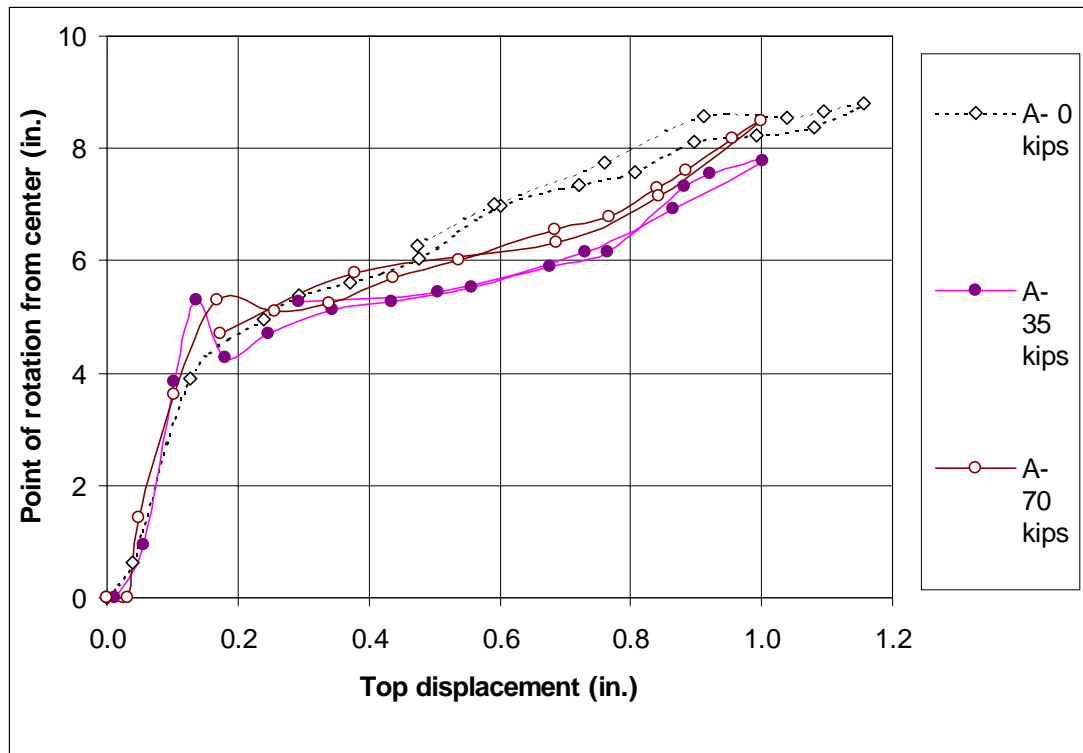


Figure 4.18. Comparison of lateral load/displacement relations of Specimens B and C



**Figure 4.19.** Bending strains measured on dowels of Specimen C



**Figure 4.20.** Point of rotation of Specimen A during static load tests

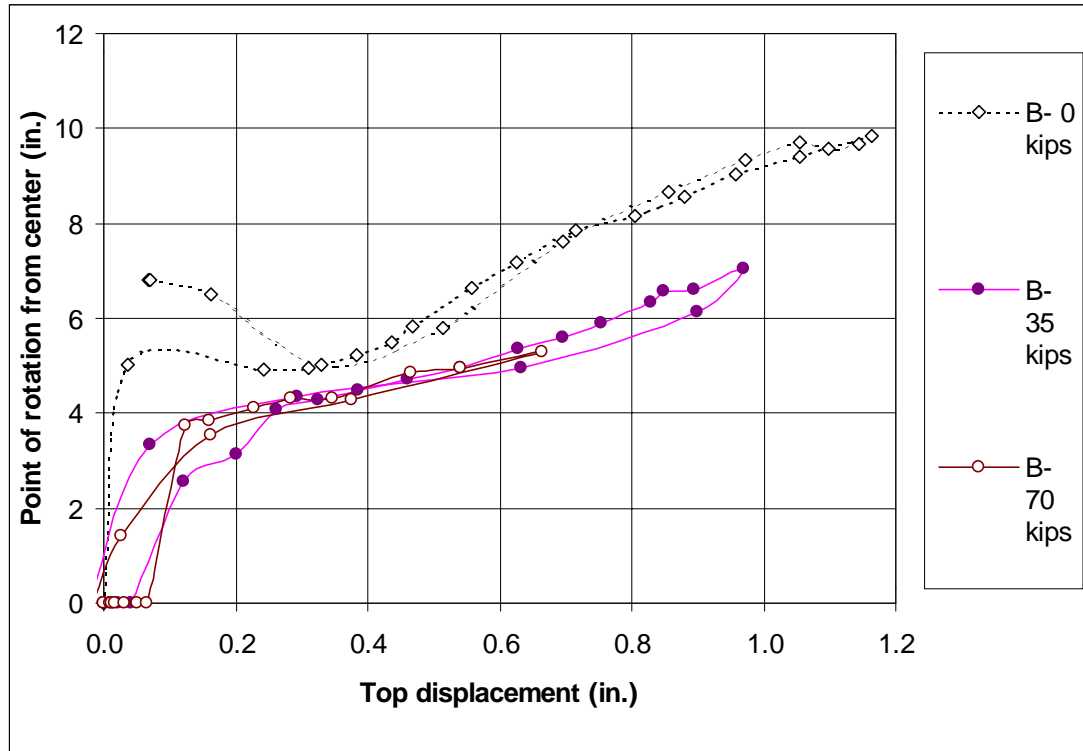


Figure 4.21. Point of rotation of Specimen B during static load tests

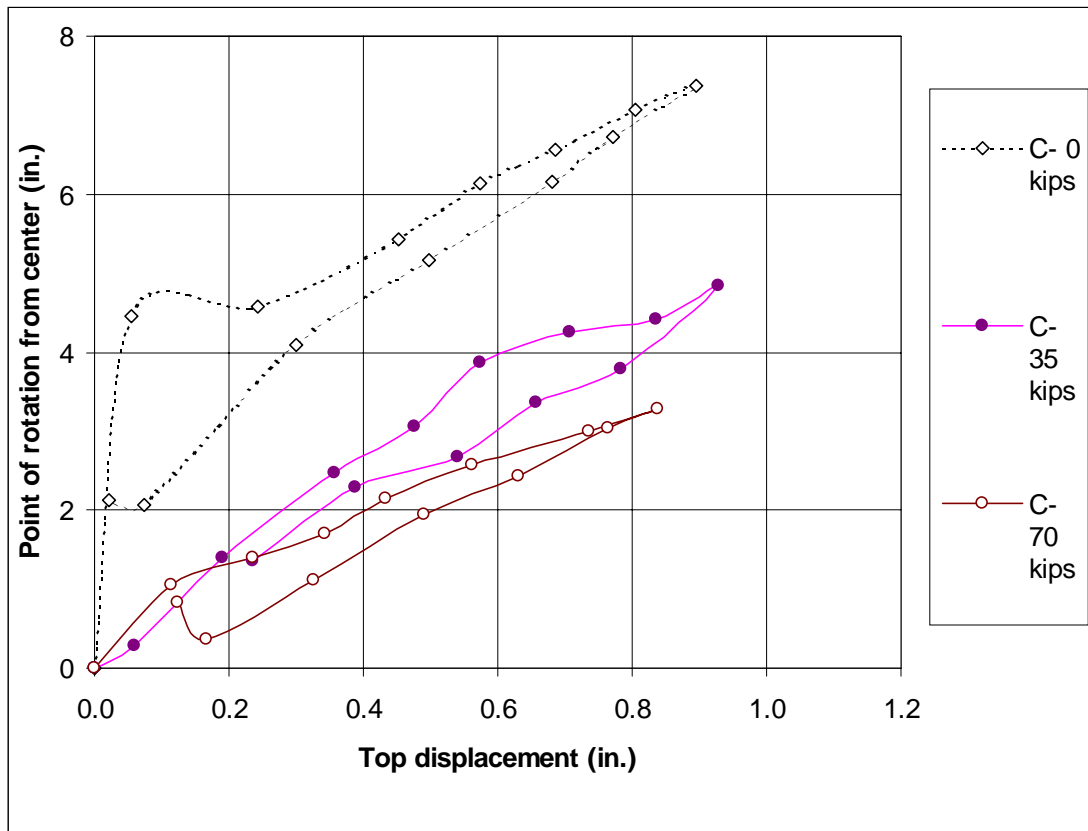
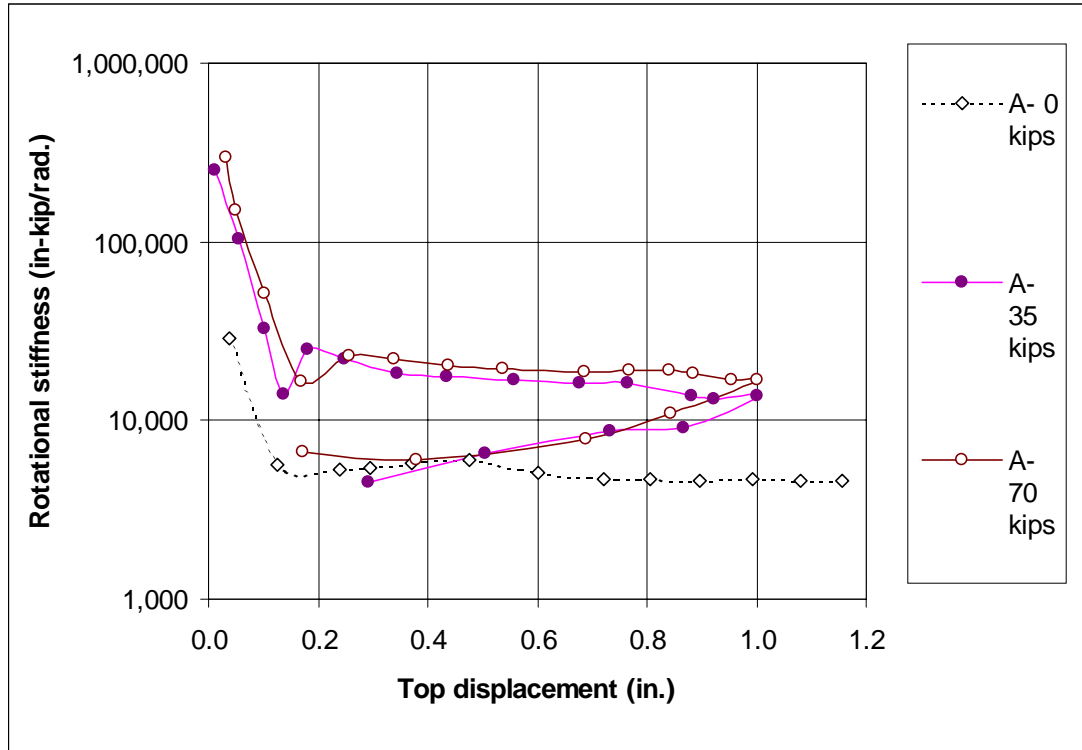


Figure 4.22. Point of rotation of Specimen C during static load tests



**Figure 4.23.** Rotational stiffness of Specimen A during static load tests

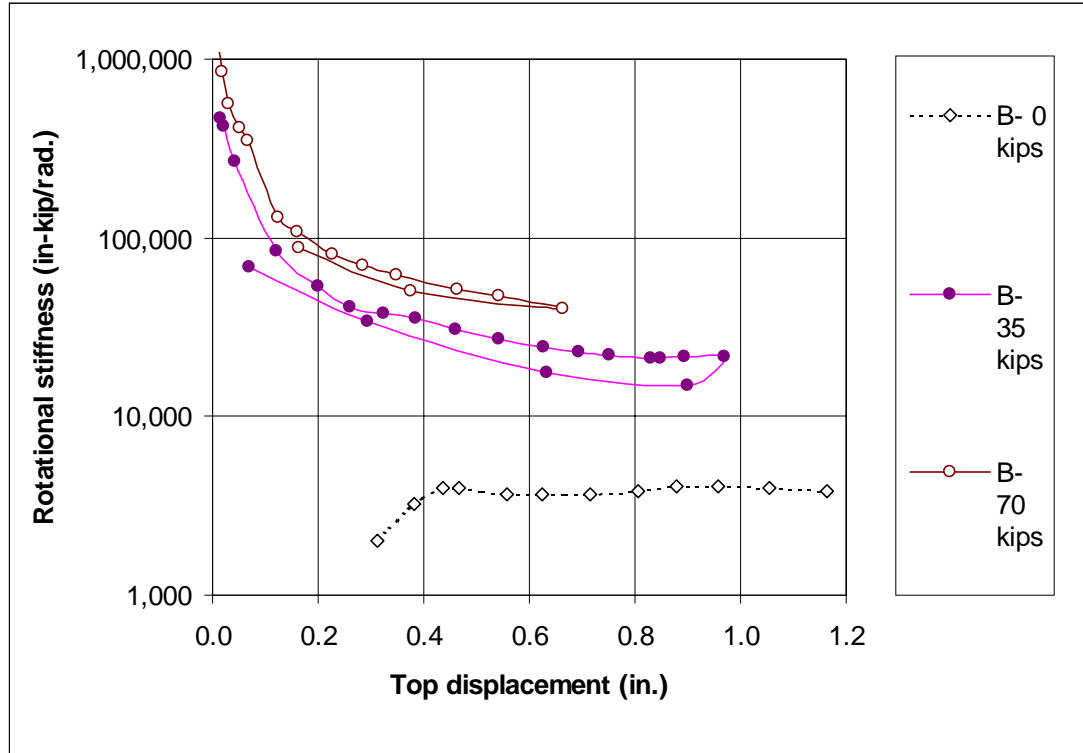


Figure 4.24. Rotational stiffness of Specimen B during static load tests

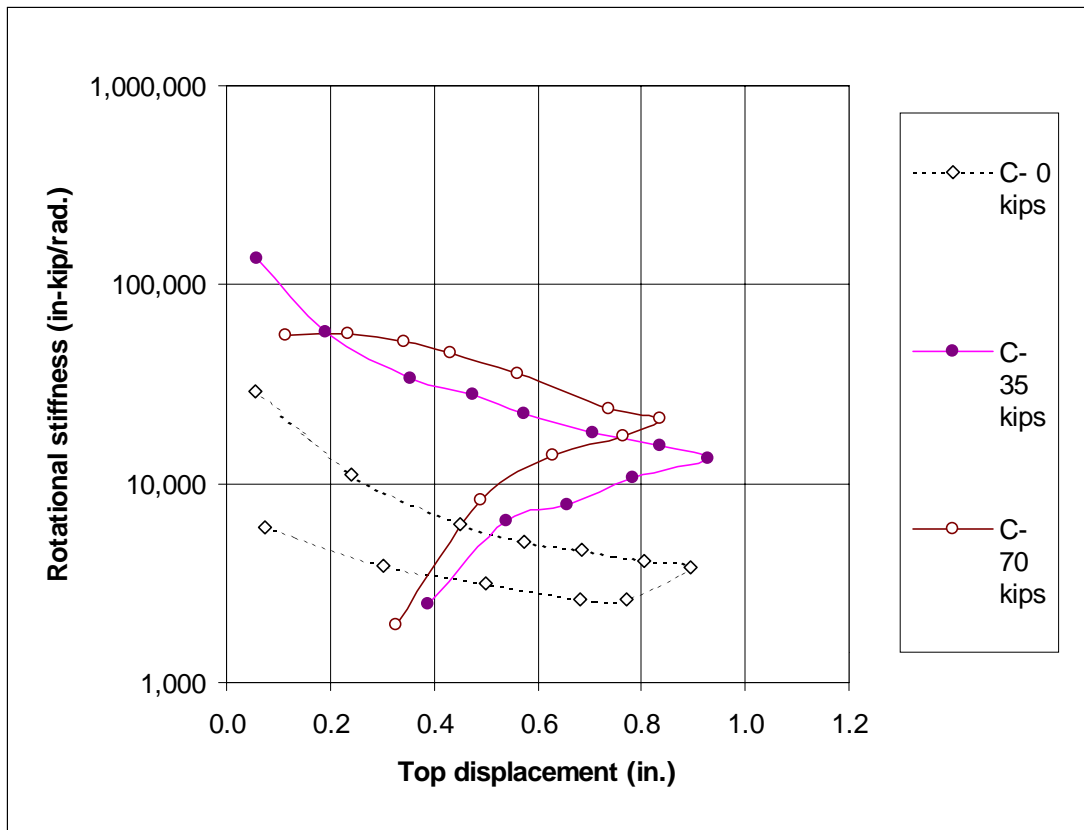
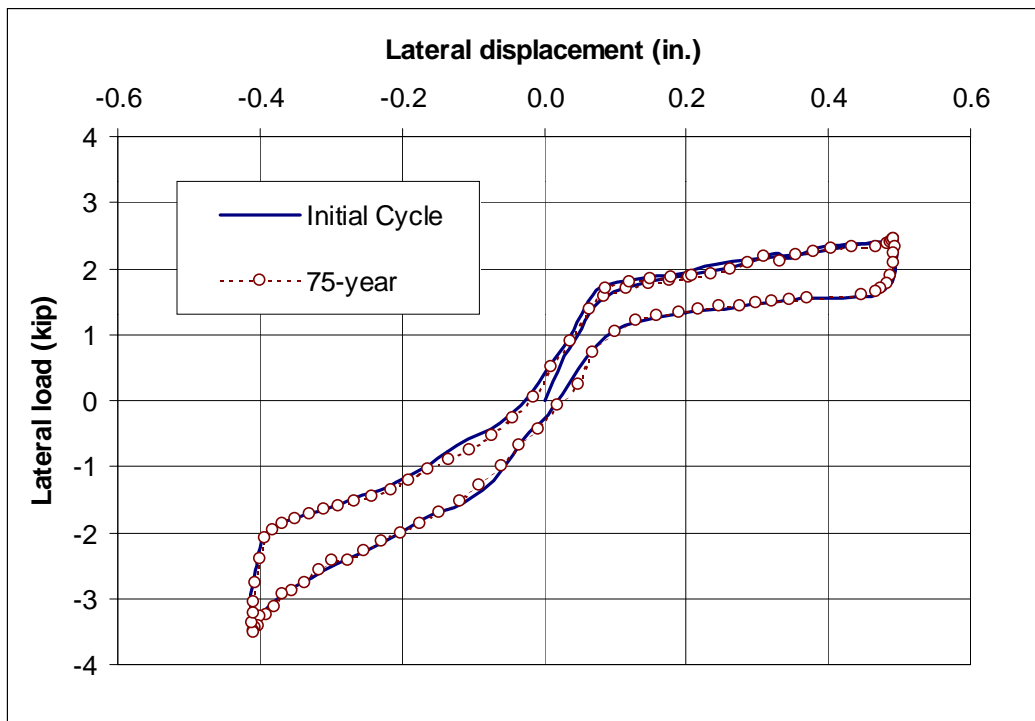
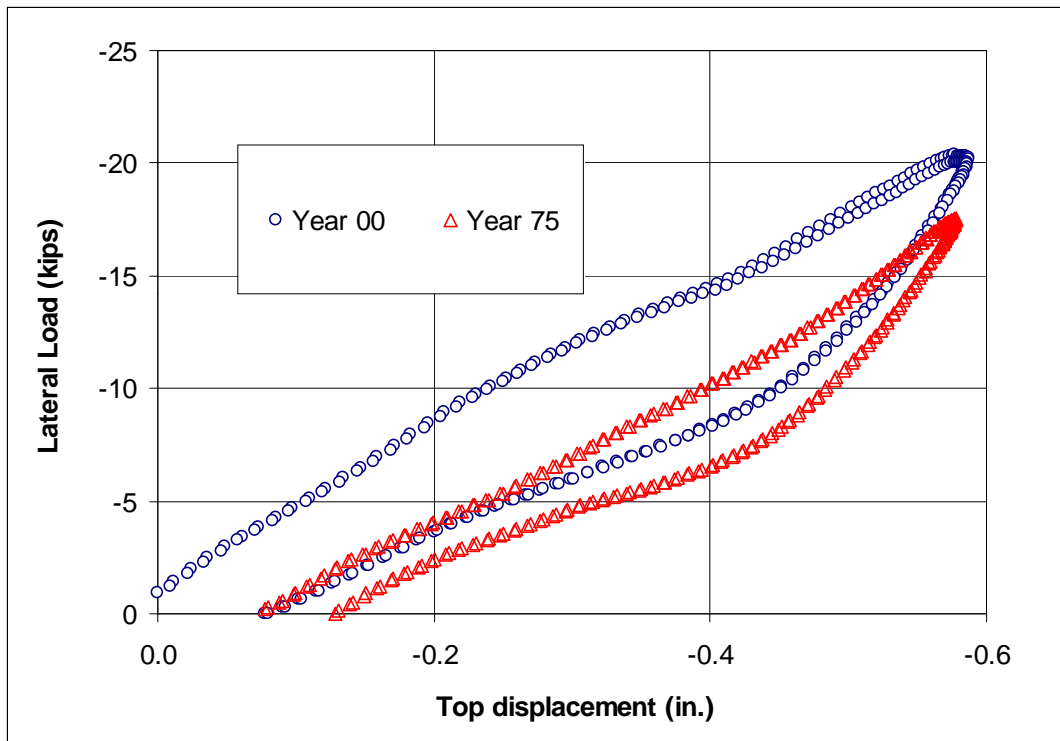


Figure 4.25. Rotational stiffness of Specimen C during static load tests



**Figure 4.26.** Lateral load/displacement relationship of Specimen B for zero vertical load during cyclic tests



**Figure 4.27.** Lateral load/displacement relationship of Specimen B for 35-kip vertical load during cyclic tests

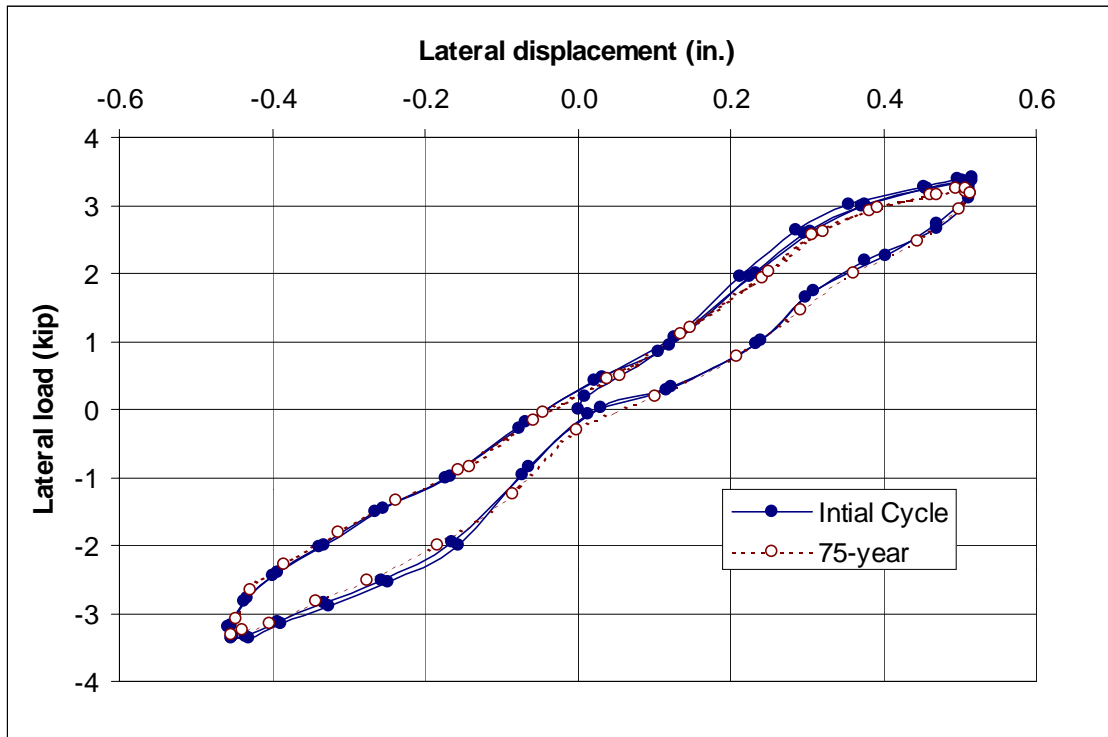


**Figure 4.28.** Lateral load/displacement relationship of Specimen C for zero vertical load during cyclic tests

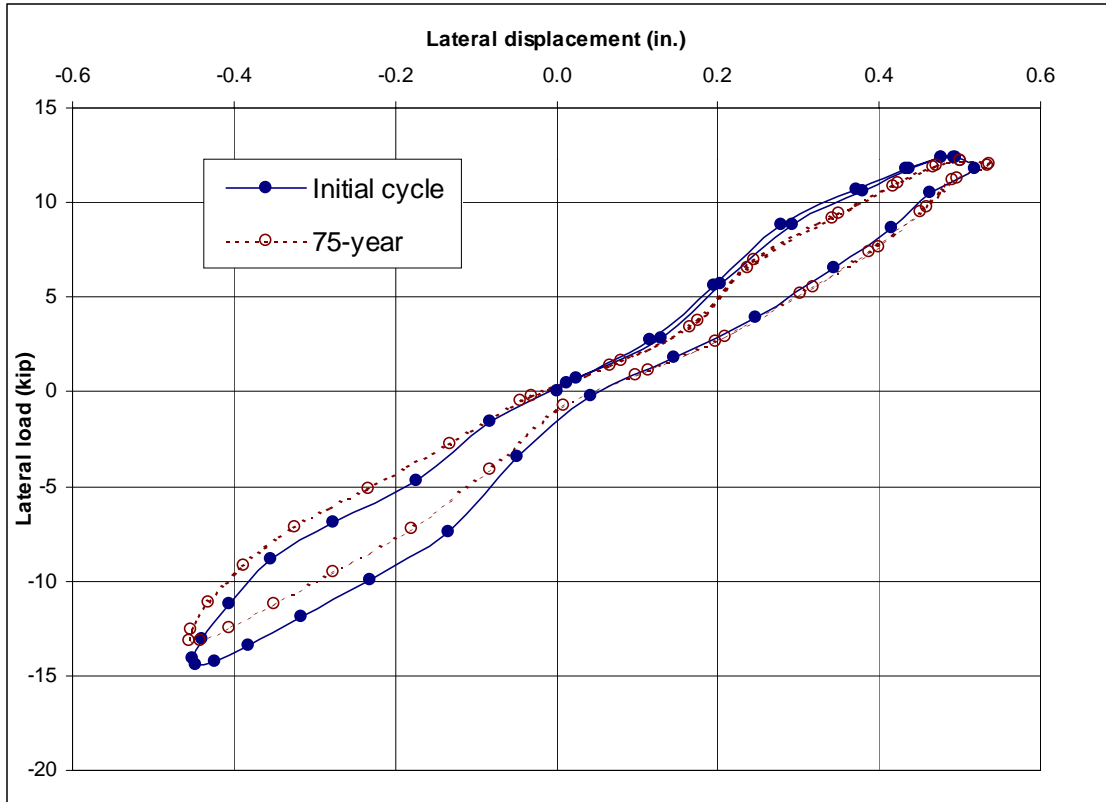


**Figure 4.29.** Lateral load/displacement relationship of Specimen C for 35-kip vertical load during cyclic tests

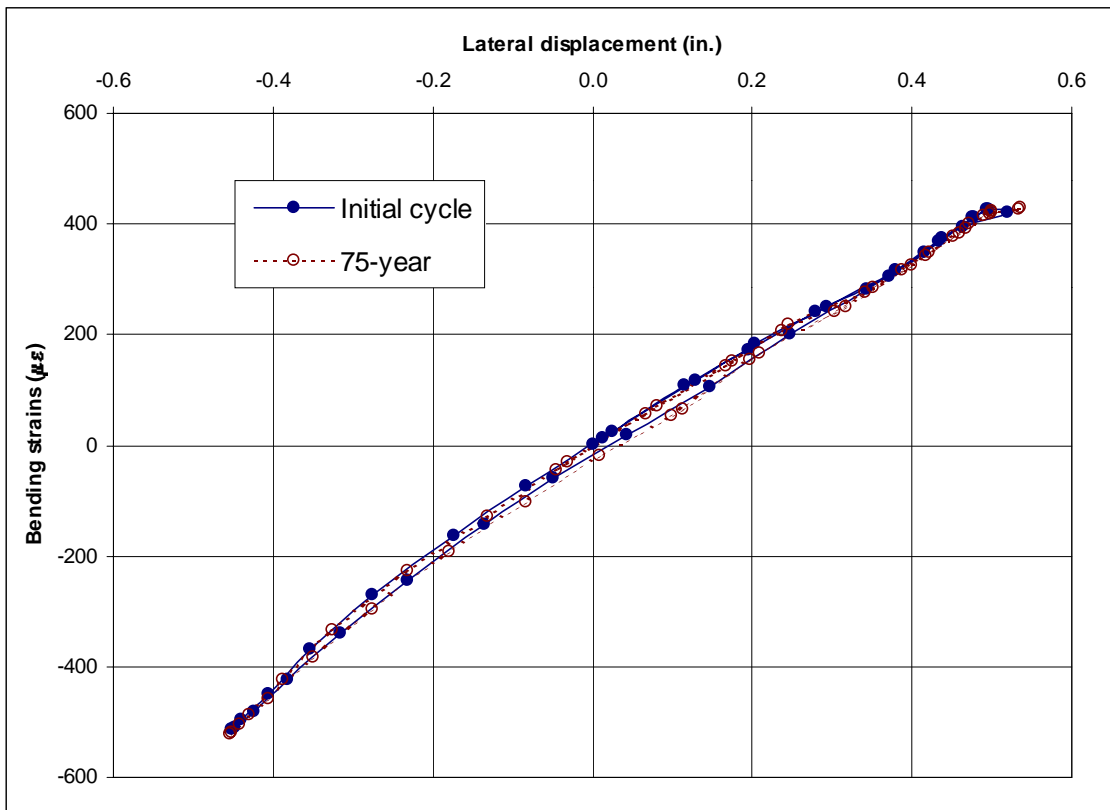


**Figure 4.30.** Bending strain/displacement relationship of Specimen C for zero vertical load during cyclic tests

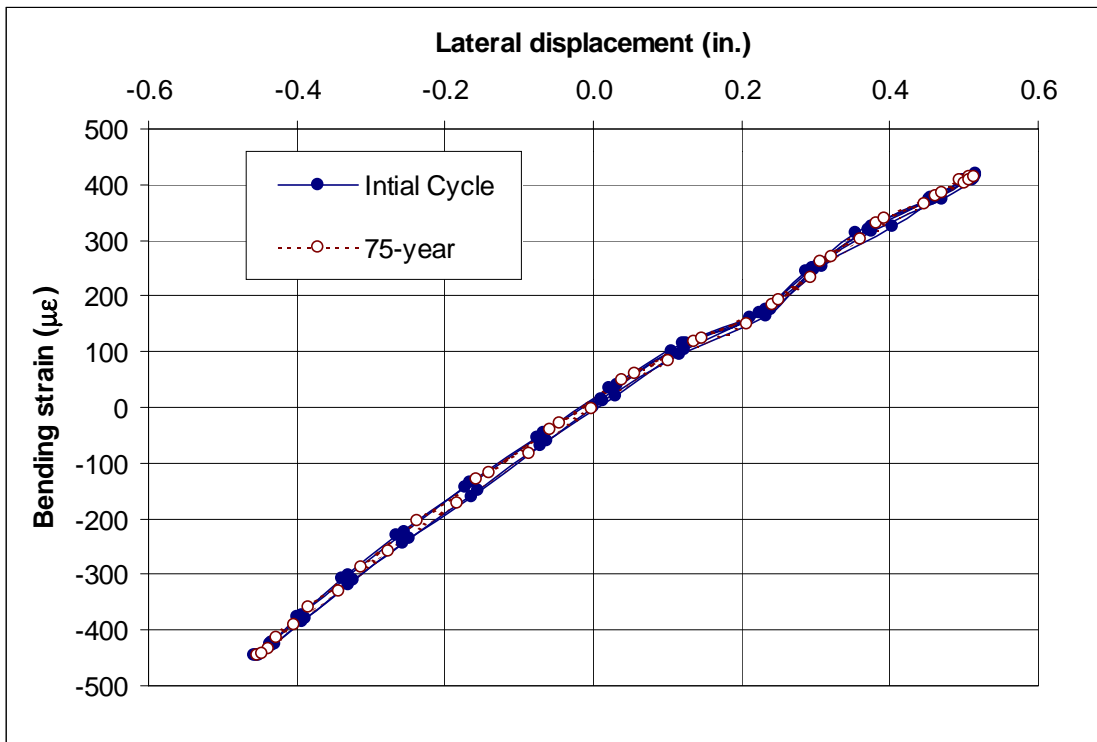


**Figure 4.31.** Bending strain/displacement relationship of Specimen C for 35-kip vertical load during cyclic tests

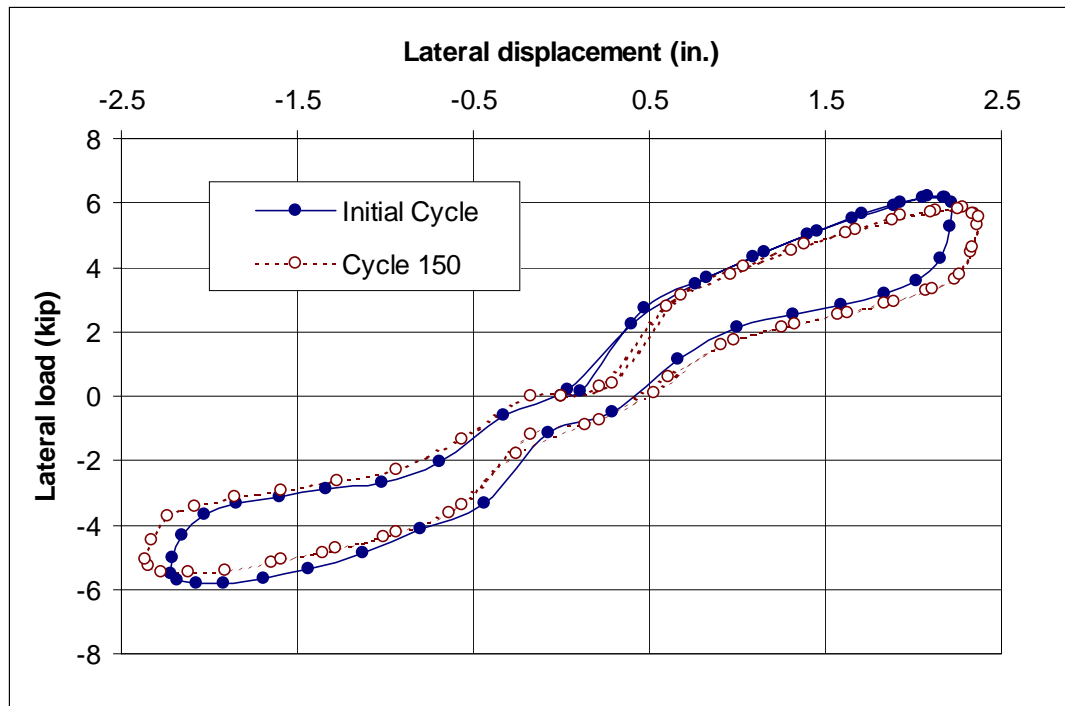


**Figure 4.32.** Lateral load/displacement relationship of Specimen C for zero vertical load during large displacement cyclic tests

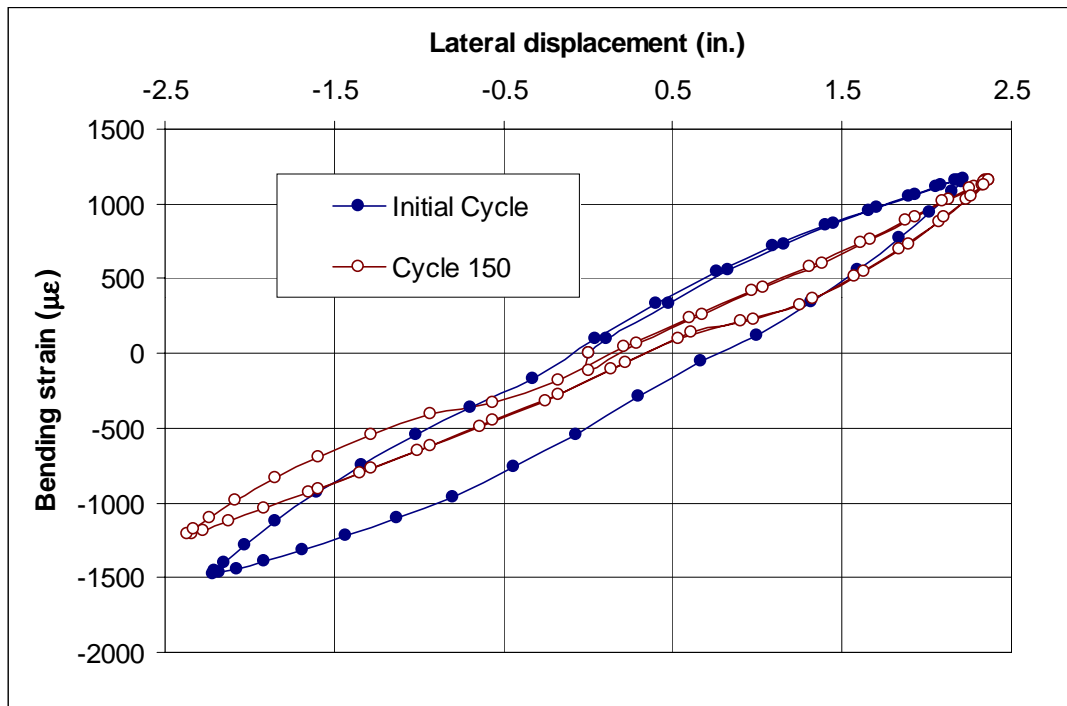


**Figure 4.33.** Bending strain/displacement relationship of Specimen C for zero vertical load during large displacement cyclic tests